City, University of London Institutional Repository

This is the accepted version of the paper.

This version of the publication may differ from the final published version.

WILEY

Publishers Since 1807

111 RIVER STREET, HOBOKEN, NJ 07030

IMMEDIATE RESPONSE REQUIRED

Your article will be published online via Wiley's EarlyView® service (wileyonlinelibrary.com) shortly after receipt of corrections. Articles posted online in EarlyView® are peer-reviewed, copyedited, author corrected, and fully citable via the article DOI (for further information, visit www.doi.org). EarlyView® means you benefit from the best of two worlds--fast online availability as well as traditional, issue-based archiving.

☐ **READ PROOFS CAREFULLY**

- This will be your only chance to review these proofs. Please note that once your corrected article is posted online, it is considered legally published, and cannot be removed from the Web site for further corrections.

- Please note that the volume and page numbers shown on the proofs are for position only.

☐ **ANSWER ALL QUERIES ON PROOFS**

- Please annotate all corrections and remember to respond to all author queries at the back of your page proofs.

☐ **CHECK FIGURES AND TABLES CAREFULLY**

- Check size, numbering, and orientation of figures.
- All images in the PDF are downsampled (reduced to lower resolution and file size) to facilitate Internet delivery. These images will appear at higher resolution and sharpness in the printed article.
- Review figure legends to ensure that they are complete.
- Check all tables. Review layout, title, and footnotes.

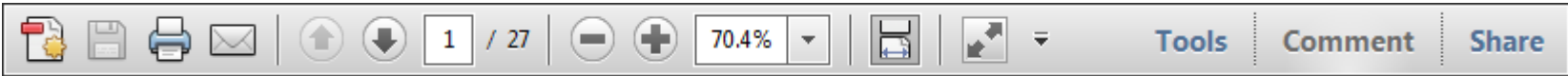**RETURN**   ☐ **CORRECTED PROOFS**
☐ **Other forms as needed**

The preferred method to return corrected proofs is to return the annotated PDF to jrnlprodjbma@cadmus.com.

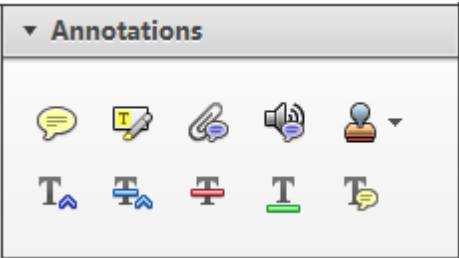**RETURN ALL RELEVANT ITEMS WITHIN 48 HOURS OF RECEIPT**

USING e-ANNOTATION TOOLS FOR ELECTRONIC PROOF CORRECTION

Required software to e-Annotate PDFs: Adobe Acrobat Professional or Adobe Reader (version 7.0 or above). (Note that this document uses screenshots from Adobe Reader X)
The latest version of Acrobat Reader can be downloaded for free at: http://get.adobe.com/uk/reader/

Once you have Acrobat Reader open on your computer, click on the Comment tab at the right of the toolbar:

| 📄 💾 🖨 ✉ | ⬆ ⬇ 1 / 27 ⊖ ⊕ 70.4% ▾ | 💾 ⤢ ▾ | Tools | Comment | Share |

This will open up a panel down the right side of the document. The majority of tools you will use for annotating your proof will be in the Annotations section, pictured opposite. We've picked out some of these tools below:
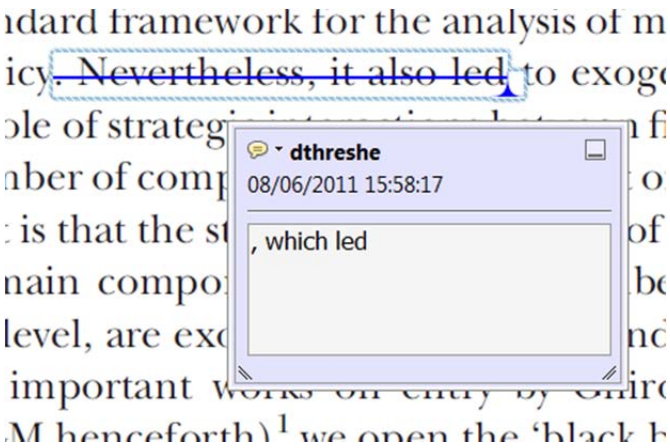
▾ Annotations

---

1. Replace (Ins) Tool – for replacing text.

Strikes a line through text and opens up a text box where replacement text can be entered.

How to use it

- Highlight a word or sentence.
- Click on the Replace (Ins) icon in the Annotations section.
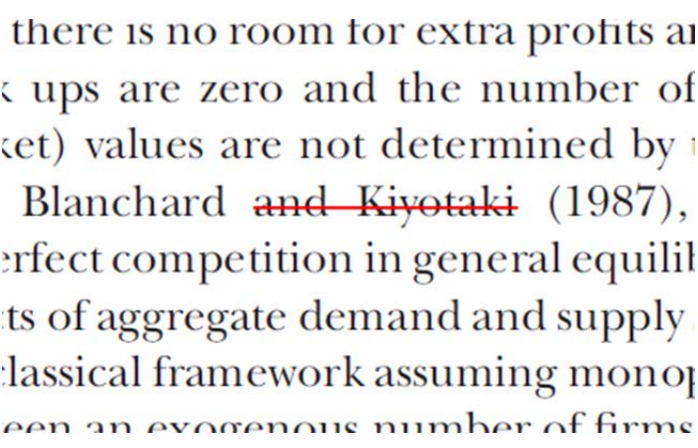- Type the replacement text into the blue box that appears.

ıdard framework for the analysis of m
icy. Nevertheless, it also led to exoga
ole of strategi~~c~~
~~ıber of comp~~
~~: is that the st~~
~~ıain compo~~
~~level, are exa~~
important wo~~~~
.M henceforth)[1] we open the 'black h

dthreshe
08/06/2011 15:58:17

, which led

---

2. Strikethrough (Del) Tool – for deleting text.

Strikes a red line through text that is to be deleted.

How to use it

- Highlight a word or sentence.
- Click on the Strikethrough (Del) icon in the Annotations section.

. there is no room for extra profits a
: ups are zero and the number of
et) values are not determined by
Blanchard ~~and Kiyotaki~~ (1987),
:rfect competition in general equili
ts of aggregate demand and supply
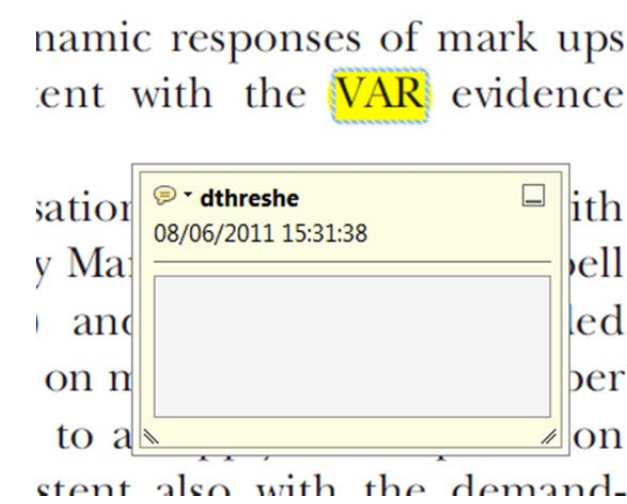lassical framework assuming monoj
een an exogenous number of firms

---

3. Add note to text Tool – for highlighting a section to be changed to bold or italic.

Highlights text in yellow and opens up a text box where comments can be entered.

How to use it

- Highlight the relevant section of text.
- Click on the Add note to text icon in the Annotations section.
- Type instruction on what should be changed regarding the text into the yellow box that appears.

namic responses of mark ups
ent with the **VAR** evidence

sation
y Ma
and
on r
to a
stent also with the demand-

dthreshe
08/06/2011 15:31:38

---

4. Add sticky note Tool – for making notes at specific points in the text.

Marks a point in the proof where a comment needs to be highlighted.

How to use it

- Click on the Add sticky note icon in the Annotations section.
- Click at the point in the proof where the comment should be inserted.
- Type the comment into the yellow box that appears.

ıand and supply shocks. Most oı
a~~ami~~
numbe
dard fr
icy. Nev
ole of st
ıber of competitors and the imp
is that the structure of the secto

dthreshe
08/06/2011 15:18:08

USING e-ANNOTATION TOOLS FOR ELECTRONIC PROOF CORRECTION

5. Attach File Tool – for inserting large amounts of text or replacement figures.

Inserts an icon linking to the attached file in the appropriate pace in the text.

How to use it
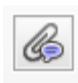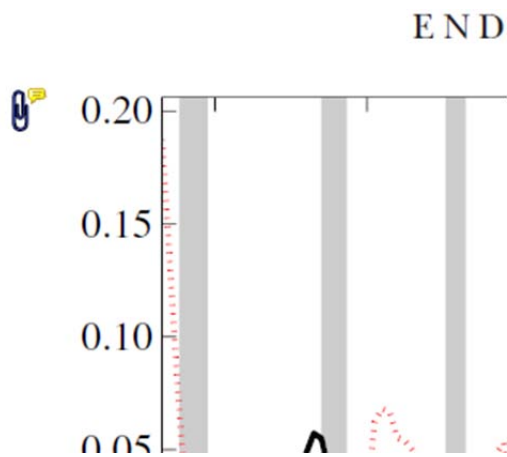
- Click on the Attach File icon in the Annotations section.
- Click on the proof to where you'd like the attached file to be linked.
- Select the file to be attached from your computer or network.
- Select the colour and type of icon that will appear in the proof. Click OK.

6. Add stamp Tool – for approving a proof if no corrections are required.

Inserts a selected stamp onto an appropriate place in the proof.

How to use it

- Click on the Add stamp icon in the Annotations section.
- Select the stamp you want to use. (The Approved stamp is usually available directly in the menu that appears).
- Click on the proof where you'd like the stamp to appear. (Where a proof is to be approved as it is, this would normally be on the first page).

7. Drawing Markups Tools – for drawing shapes, lines and freeform annotations on proofs and commenting on these marks.

Allows shapes, lines and freeform annotations to be drawn on proofs and for comment to be made on these marks..

How to use it

- Click on one of the shapes in the Drawing Markups section.
- Click on the proof at the relevant point and draw the selected shape with the cursor.
- To add a comment to the drawn shape, move the cursor over the shape until an arrowhead appears.
- Double click on the shape and type any text in the red box that appears.

For further information on how to annotate proofs, click on the Help menu to reveal a list of further options:

WILEY-BLACKWELL

Additional reprint purchases

Should you wish to purchase additional copies of your article, please click on the link and follow the instructions provided:
https://caesar.sheridan.com/reprints/redir.php?pub=10089&acro=JBMA

Corresponding authors are invited to inform their co-authors of the reprint options available.

Please note that regardless of the form in which they are acquired, reprints should not be resold, nor further disseminated in electronic form, nor deployed in part or in whole in any marketing, promotional or educational contexts without authorization from Wiley. Permissions requests should be directed to mail to: permissionsus@wiley.com

For information about 'Pay-Per-View and Article Select' click on the following link: wileyonlinelibrary.com/aboutus/ppv-articleselect.html

WILEY
Publishers Since 1807

COLOR REPRODUCTION IN YOUR ARTICLE

Color figures were included with the final manuscript files that we received for your article. Because of the high cost of color printing, we can only print figures in color if authors cover the expense.

Please indicate if you would like your figures to be printed in color or black and white. Color images will be reproduced online in *Wiley Online Library* at no charge, whether or not you opt for color printing.

You will be invoiced for color charges once the article has been published in print.

Failure to return this form with your article proofs will delay the publication of your article.

JOURNAL   **Journal of Biomedical Materials Research**

MS. NO.   NO. OF COLOR PAGES

TITLE OF MANUSCRIPT

AUTHOR(S)

Color Pages	1 Figure per Page	2 Figures per Page	3 Figures per Page	4 Figures per Page	5 Figures per Page	6 Figures per Page
1	850	1000	1150	1300	1450	1600
2	1700	1850	2000	2150	2300	2450
3	2550	2700	2850	3000	3150	3300
4	3400	3550	3700	3850	4000	4150
5	4250	4400	4550	4700	4850	5000
6	5100	5250	5400	5550	5700	5850

Please contact the Production Editor at jrnlprodjbma@cadmus.com for a quote if you have more than 6 pages of color

---

☐   Please print my figures in black and white

☐   Please print my figures in color $ _____

**International orders must be paid in currency and drawn on a U.S. bank

BILL TO:
Name _____

Institution _____

Address _____

_____

_____

Purchase Order No. _____

Phone _____

_____

Fax _____

E-mail _____

Society For Biomaterials

Permeability of rapid prototyped artificial bone scaffold structures

AQ3   Marcin Lipowiecki,[1,2] Markéta Ryvolová,[1,2,3] Ákos Töttösi,[1,2] Niels Kolmer,[1,2] Sumsun Naher,[1,2,4]
AQ2   Stephen Brennan,[5] Mercedes Vázquez,[1,2,6] Dermot Brabazon[1,2,5]

[1]School of Mechanical and Manufacturing Engineering, Dublin City University, Glasnevin, Dublin 9, Ireland
[2]Advanced Processing Technology Research Centre, Dublin City University, Dublin 9, Ireland
[3]Department of Chemistry, Faculty of Science, Masaryk University, Kotlářská 2, Brno, Czech Republic
[4]School of Engineering and Mathematical Sciences, City University London, London, United Kingdom
AQ4   [5]University College Hospital Galway, Galway, Ireland
[6]Irish Separation Science Cluster (ISSC), National Centre for Sensor Research, Dublin City University, Dublin 9, Ireland

Abstract: In this work, various three-dimensional (3D) scaffolds were produced via micro-stereolithography (μ-SLA) and 3D printing (3DP) techniques. This work demonstrates the advantages and disadvantages of these two different rapid prototyping methods for production of bone scaffolds. Compared to 3DP, SLA provides for smaller feature production with better dimensional resolution and accuracy. The permeability of these structures was evaluated experimentally and via numerical simulation utilizing a newly derived Kozeny–Carman based equation for intrinsic permeability. Both experimental and simulation studies took account of porosity percentage, pore size, and pore geometry. Porosity content was varied from 30% to 70%, pore size from 0.34 mm to 3 mm, and pore geometries of cubic and hexagonal closed packed were examined. Two different fluid viscosity levels of 1 mPa s and 3.6 mPa s were used. The experimental and theoretical results indicated that permeability increased when larger pore size, increased fluid viscosity, and higher percentage porosity were utilized, with highest to lowest degree of significance following the same order. Higher viscosity was found to result in permeabilities 2.2 to 3.3 times higher than for water. This latter result was found to be independent of pore morphology type. As well as demonstrating method for determining design parameters most beneficial for scaffold structure design, the results also illustrate how the variations in patient's blood viscosity can be extremely important in allowing for permeability through the bone and scaffold structures. © 2014 Wiley Periodicals, Inc. J Biomed Mater Res Part A: 00A:000–000, 2014.

Key Words: permeability, synthetic scaffold, tissue engineering, trabecular bone, rapid prototyping

How to cite this article: Lipowiecki M, Ryvolová M, Töttösi Á, Kolmer N, Naher S, Brennan S, Vázquez M, Brabazon D. 2014. Permeability of rapid prototyped artificial bone scaffold structures. J Biomed Mater Res Part A 2014:00A:000–000.

INTRODUCTION

Synthetic bone scaffolds are used during surgery to aid fracture repair, replace diminished bone stock, and assist osseointegration of orthopedic implants to the native bone. These structures need to meet mechanical strength and permeability requirements to allow for load bearing and osteoconductivity. To increase osteoconductivity, the structure should be designed to allow for flow of nutrients and waste products related to the growth of new tissue. Fluid flow through a bone scaffold is therefore an important factor in its ability to regenerate a living tissue. Permeability is often used as a measure of a structure's ability to allow for this. There is currently a wide range of biocompatible materials available for tissue engineering including polymers, ceramics and metals.[1–4] Porous tantalum (Trabecular Metal[TM]) was characterized in the work of Shimko et al.[2,3] In their work,

scaffolds with a porosity of 66% to 88% were tested for various parameters such as tangent elastic modulus, yield stress, strain behavior, and intrinsic permeability. They concluded that the intrinsic permeability and tangent elastic modulus of tantalum correspond well with those of cancellous bones of similar porosity. Whereas ceramic and metal based scaffold materials are used for hard tissue scaffolds, polymer based scaffolds are used for either hard or soft tissue applications depending on the polymer type used and implant site specific requirements. Polymer-based scaffolds types were reviewed recently.[1,5] The use of poly(methyl methacrylate) in particular has been found to be suitable for the manufacturing of highly porous scaffolds with controllable elastic modulus and permeability.[2] Scaffolds developed by foaming sol–gel derived bioactive glasses were characterized by Jones et al.[6] In their work the

1

interconnectivity of pores was assessed and it was found that the permeability of the fabricated scaffolds was comparable to that of trabecular bone.

The scaffold microstructure plays an important role in cell attachment and tissue vascularization.[7] It is well known that cell ongrowth is highly dependent on the nutrients and waste product transfer through the porous structure.[8,9] Therefore, measurement of the capability of fluid to travel through the fabricated scaffold designs is an important scaffold structure characteristic. Permeability of the structure is thought to be related more to cell growth than conventionally analyzed parameters alone, for example, porosity and pore size.[7] Permeability is typically measured as water flow rate through the scaffold encased into a sealed chamber under a known hydrostatic pressure.[10]

Al-Munajjed et al.,[11] investigated the permeability and the porosity of hyaluronan–collagen scaffolds, suitable for soft tissues. Numerical calculations confirmed experimental results which indicated that porosity and permeability increased with increasing pore sizes. In their work, the three pore sizes chosen were 303, 403, and 525 µm. The test fluid media was water which was stored in a tank set at a constant height above the test specimen in order to keep the hydrostatic pressure at the top of the test sample constant. To determine the permeability constant, m, Darcy's law was used as follows:

$$m = \frac{Q * l}{h * d * t} \tag{1}$$

where Q is the volume of discharge, l is the length of sample which the fluid flows through, h is the hydrostatic pressure, d is the sample total cross-sectional area, and t is the time taken for the fluid to flow through. A more commonly used alternative measure of fluidity through scaffolds is called intrinsic permeability K (in units of m^2) and can be calculated from Darcy's law as follows:

$$K = \frac{q * l * \mu}{p * d} \tag{2}$$

where q is the volumetric flow rate, μ is the fluid viscosity, p is the pressure difference across the sample, and d and l are as per Eq. (1).[12,13]

Permeability of bones

Several experimental studies have been conducted to measure the intrinsic permeability of real bone.[8,14,15] In the work of Kohles et al.,[15] permeability values ranging between 10^{-10} m^2 and 10^{-9} m^2 in various directions though bovine distal femur were determined using water as the fluid medium. These bovine samples produced values in a range similar to that of human bone. Grimm and Williams measured permeabilities for human calcaneal trabecular bone in the range 0.40×10^{-9} m^2 to 11×10^{-9} m^2 using raw linseed oil as the fluid medium.[8] Permeability values determined in previous investigations for various types of human bone have ranged from 10^{-11} m^2 to 10^{-8} m^2.[1]

Different flow rates have been observed to occur at the different scale levels within trabecular bone structures which include intra- and intertrabecular pores. Various pore types include lacunar–canalicular pores (on the order of 0.1 µm), vascular channels (on the scale of 20 µm), and open-pore marrow space (up to 1 mm in scale). Estimation of bone permeability just through the lacunar–canalicular pores was investigated in the work of Beno et al.[14] In their work, several parallel-fibered diaphysis bone samples were used, from chick, rabbit, bovine, horse, dog and human origin. The number of canaliculi emanating from an osteocyte lacuna was determined and the local intrinsic permeability was estimated, using microstructural measurements. The authors provided measurements of intrinsic permeability along three axes, proving that these bone samples were anisotropic, as has previously been found for bovine bone by other workers.[15] It was also shown that that the permeability was very sensitive to canalicular and osteocytic dimensions, less sensitive to the fiber matrix spacing and strongly dependent on the type of animal tissue being studied.[14,15]

The effect of cyclical mechanical loading on fluid flow rate has been investigated using an *ex vivo* ovine model.[16] The fluid flow, which was monitored via applied color tracers, showed that mechanical load enhanced the molecular transport and that diffusion alone could efficiently transport small (300–400 Da) but not larger molecules. Previous work has also shown that cyclical loading of human bone structures can affect blood content and, in turn, bone shear strength.[17] Permeability can be seen as important therefore not only for osteoconductivity but also for the strength of bone structures.

Mathematical calculation and experimental determination of intrinsic permeability based on the tetrakaidecahedral unit has been previously presented.[18,19] Permeability was found, both experimentally and mathematically, to increase with increased pore size, and porosity. A similar technique was used in the work of Malachanne et al.[20] The aim of their work was to compare the intrinsic permeability determined by experimental measurement with their developed finite element model. The experimental measurements for validation in their work were recorded with *ex vivo* ox bone. The experimental setup consisted of a standing pipe with storage water held at a set height above the test sample producing a constant hydrostatic pressure. The time for a defined volume of water to pass through the sample was measured. An intrinsic permeability of $K = 1.1 \times 10^{-2}$ m^2 was determined.[20] Swider et al.[21] used magnetic resonance imaging to determine the fluid flow velocity, distribution, and permeability in a porous material. Their investigation was focused on hydroxyapatite bone scaffolds and the intrinsic permeability coefficient was calculated using Darcy's law, resulting in a value of $K = 2.66 \times 10^{-2}$ m^2.

Fabrication and permeability testing methods for artificial scaffolds

Although some works indicate that simulating natural healthy bone geometry is best for scaffold structures, others indicate that larger pore sizes are preferable within the
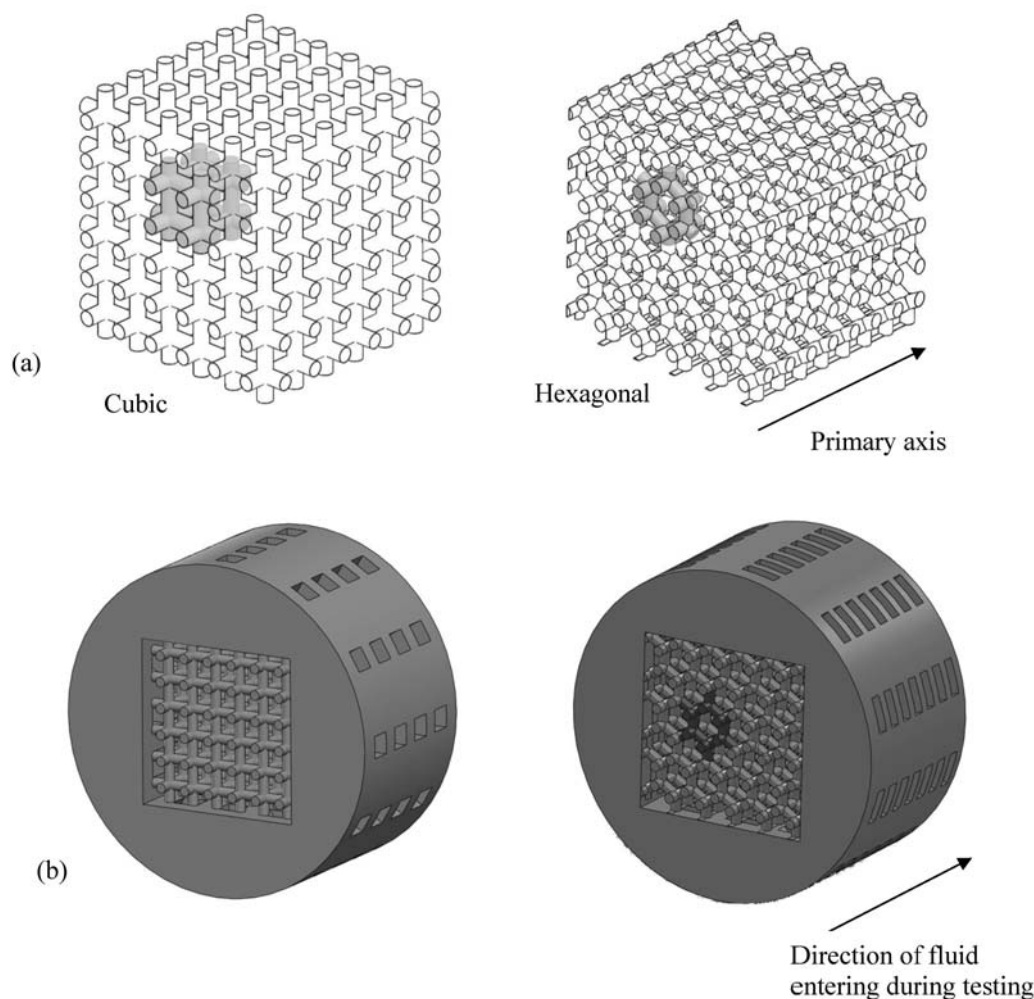
FIGURE 1. Schematics of cubic and hexagonal structures for permeability testing in isometric view shown (a) without and (b) with supporting collar. [Color figure can be viewed in the online issue, which is available at wileyonlinelibrary.com.]

AQ6

structure to allow for ingrowth of native bone and for enhanced fluid transport during the short to medium term healing process after implantation. Fluids used for this type of analysis often differ between various research groups. Usually water solutions are used[3]; however, gases have also been examined. For example, in the work of Chor and Li[7] dry air was used as the fluid medium to avoid scaffold hydrolysis and pore blockage.

Despite this previous work, the optimal method of testing, fabrication method, and pore geometry is still undecided. In order to advance the knowledge in this area, the work presented in this article was undertaken using two different well defined structure types, cubic and hexagonal close packed. These were fabricated by stereolithography (SLA) and three-dimensional (3D) printing (3DP). A great amount of interest within the last 10 years has focused on the use of rapid prototyping to manufacture synthetic bone scaffolds.[23–25] Structures produced by rapid prototyping techniques, allow for control of pore size, porosity, and geometry. These structures have previously been tested by the authors and confirmed to be suitable to withstand the

mechanical loading requirements of bone scaffolds.[26,27] These structure types provide a high stiffness and, at the same time, a high level of porosity and large pore size which would be considered advantageous for achieving a high level of permeability. The aim of this work therefore was to investigate the use of SLA and 3DP rapid prototyping methods for the production of predefined, previously stress-tested, cubic, and hexagonal synthetic bone scaffold designs with a view to optimizing these for permeability.

MATERIALS AND METHODS
Experimental permeability testing
The scaffold model structures were designed using computer aided design software SolidEdge V100 and saved as SLA files. Two basic structures, hexagonal and cubic, were fabricated, see Figure 1. The set pore size and porosity percentage are summarized in Table I. The cubic structure was omnidirectional and therefore was tested along only one axis. The hexagonal structure has one primary axis in which fluid can flow with least obstruction (shown in Fig. 1). The fluid flow tests were performed along this direction. The

F1

T1

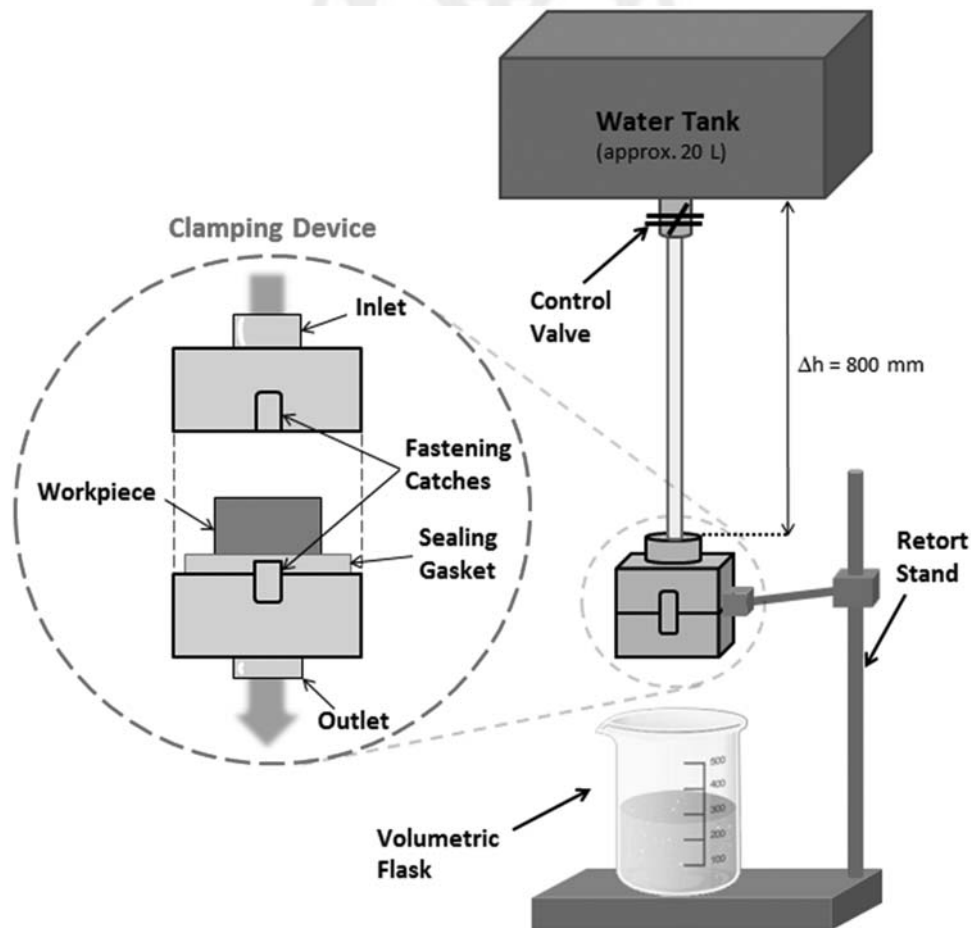**TABLE I. Summary of the Porosities and Pore Sizes Investigated for Each Cubic and Hexagonal Structure**

Target Pore Size (mm)	Porosity		
	30%	50%	70%
0.34	C	–	–
0.6	C/H	C	–
1.5	C/H	C/H	C/H
2	C/H	C/H	C/H
2.5	C/H	C/H	C/H
3	C/H	C/H	C/H

C, cubic; H, hexagonal.

majority of samples were manufactured using a Z310 Z-Corp 3D printer with standard 3DP plaster powder material ZP113 and binder ZB-58. To reinforce the specimens, they were infiltrated using epoxy ZMax resin and left overnight to dry. Biocompatibility of these materials was not sought or required for the current work as this article focuses on permeability assessment of different structure geometries and scales. A micro-SLA (μ-SLA) high definition ProJet™ MP 7000, 3DSystems, was used to produce the smallest samples and some samples of similar size to the 3D printed

scaffolds for comparison. These models were fabricated with commercial Accura 60 resin.

Samples with six different scaffold pore sizes set in the range from 0.34 mm to 3 mm and porosity percentages of 30%, 50%, and 70% were fabricated by these methods. This resulted in 15 different cubic and 13 different hexagonal scaffold pore size/percentage combinations being fabricated, see Table I. Triplicates of each sample type were fabricated and flow rate through each sample was measured three times in order to allow for repeatability analysis. This resulted in nine flow rate measurements for each of the scaffold geometries. In this work the model pore size was defined as the inner length of the edges of the cubes for the cubic structures, and as the minimum diameter of an inner circle which could be contained within the hexagonal structures. For the hexagonal structures, the height of the repeated units was also recorded in order to fully define these lattice structures. The boundary of the scaffold structures was a 15 mm × 15 mm × 15 mm for pore sizes from 1.5 mm to 3.0 mm and a 3 mm × 3 mm × 3 mm for pore sizes from 0.34 mm to 0.60 mm. A solid outer shell was built into the model to house these scaffold structures and to fit into the clamping device for permeability

FIGURE 2. Schematic of the setup for synthetic bone scaffold permeability measurement. [Color figure can be viewed in the online issue, which is available at wileyonlinelibrary.com.]

measurement, see Figure 1. The permeability testing rig is shown in Figure 2. This cylindrical collar around the scaffold structures served as a sealing surface with the clamping device walls. The printing time for 10 samples with a 3-mm pore size was about 30 min and for 10 samples with a 1.5 mm pore size the printing time was about 90 min.

Two liquids with different viscosities (water and water with 30% glycerol solution) were tested. The water–glycerol solution (Sigma Aldrich) was used as a basic simulation of higher viscosity blood fluid, the viscosity of which is in the range of three to six times higher than water depending on the hematocrit, blood flow rate, and blood constituents such as proteins, nutrients, hormones, and excretory products. Blood typically varies from 3 mPa s to 6 mPa s while blood without cells typically varies from 1 mPa s to 1.3 mPa s.[28,29] In this work, the viscosity of the water and water–glycerol solution used were recorded using a rotational viscometer (Rheology International Instrument, ASTM Spindle Type2) at 1 mPa s and 3.6 mPa s, respectively. In order to understand the influence of the sample material on the flow, the contact angles of three different fluids, that is, tap water, deionized water, and water–glycerol solution (30% glycerol by mass), were measured with a FTA-200 dynamic contact angle analyzer.

The fluid holding tank contained a measured volume of 20 L. This large tank provided constant hydrostatic pressure, p, and was set at a height, Δh, of 800 mm above the sample. The hydrostatic pressure was calculated as follows:

$$p = \rho_w \ \Delta h \, g = 7833 \text{ Pa for water}$$

$$p = \rho_{g/w} \ \Delta h \, g = 8459 \text{ Pa for glycerol/water solution}$$

where $\rho_w = 998$ kg/m^3 and $\rho_{g/w} = 1077$ kg/m^3 at 20°C. In order to conduct each permeability test, the specimen was placed into the clamping device and the time required for 500 mL of fluid to pass into the graduated container was measured. Darcy's law, according to Eq. (2), was then used to calculate the experimentally determined intrinsic permeability values.

Mathematical modeling of permeability

Packed bed models are widely used in industry to calculate the pressure drop of a fluid flowing through a packed bed of solids. Such models have often been used to determine the permeability of scaffolds.[6] The Kozeny–Carman equation, first proposed by Kozeny and later refined by Carman, is commonly used to predict permeability in various solids.[30–33] This equation has many forms and is based on classical Navier–Stokes fluid mechanics. The Kozeny–Carman equation can be expressed to give n, the hydraulic conductivity (m/s), as follows:

$$n = C \times \frac{g}{\mu_w \, \rho_w} \times \frac{e^3}{S^2 \, D_r^2 \, (1+e)} \tag{3}$$

where C, constant; μ_w, dynamic viscosity of water [Ps.s]; ρ_w, density of fluid [kg/m^3]; e, void ratio; g, acceleration of gravity [m/s^2]; S, specific surface area $\left[\frac{\text{m}^2}{\text{kg}}\right]$; $D_r = \frac{\text{density of solid}}{\text{density of fluid}}$.

Given that

$$n = K \, \frac{\rho_w \, g}{\mu_w} \tag{4}$$

where K is the intrinsic permeability (in m^2), the Kozeny–Carman equation can be rearranged to express it in terms of the intrinsic permeability:

$$=> K \, \frac{\rho_w \, g}{\mu_w} = C \, \frac{g}{\mu_w \, \rho_w} \, \frac{e^3}{S^2 \, Dr^2 \, (1+e)}$$

$$=> K = \frac{\mu_w}{\rho_w \, g} \, C \, \frac{g}{\mu_w \, \rho_w} \, \frac{e^3}{S^2 \, Dr^2 \, (1+e)}$$

we get for intrinsic permeability,

$$K = C \, \frac{1}{\rho_w^2} \, \frac{e^3}{S^2 \, Dr^2 \, (1+e)} \tag{5}$$

The constant, C, is used to take into account the morphology of the flow-through channels in a porous media. A value of 0.2 based on previous work was used for C.[30] The density of the solid was 1.21 kg/m^3 for the SLA models and 1.25 kg/m^3 for the 3DP models. The specific surface area, S, which varied with each scaffold design is one of the most critical parameters in this equation. The solid specific surface area of the structures as measured directly from corresponding CAD files was used in these calculations.

RESULTS AND DISCUSSION

Fabricated scaffold structure dimensions were generally found to be slightly larger in size for the SLA produced scaffolds and smaller for the 3DP produced scaffolds compared to the original CAD file dimensions. The resulting scaffold pore sizes are shown with corresponding permeability results in Figures 3 and 4. For the experimental work, the shortest and longest periods recorded for the fluid sample to flow though the scaffold were 3.02 s and 98.22 s, respectively. The shortest time recorded was for the SLA material, with water as fluid, the hexagonal structure, with a 1.60 mm pore size, and with 70% structural porosity. The longest time was recorded from the glycerol–water solution flowing through the SLA material with the smallest pore size of 0.53 mm, 30% porosity, and a cubic structure.

Experimental permeability testing results

Figure 3(a,b) shows the experimentally captured permeability results with water as the fluid medium for the cubic and hexagonal structures, respectively. Figure 4(a,b) shows the experimental measured permeability results with the glycerol–water solution for cubic and hexagonal structures, respectively. The range of permeabilities measured was from 1.84×10^{-10} m^2 to 4.19×10^{-9} m^2. These measurements were highly repeatable, with 95% confidence intervals being an order of magnitude less than the measured results. Thus, the plotted error bars were actually overlapped by the point markers in Figures 3 and 4. As expected, higher flow rates and permeabilities occurred
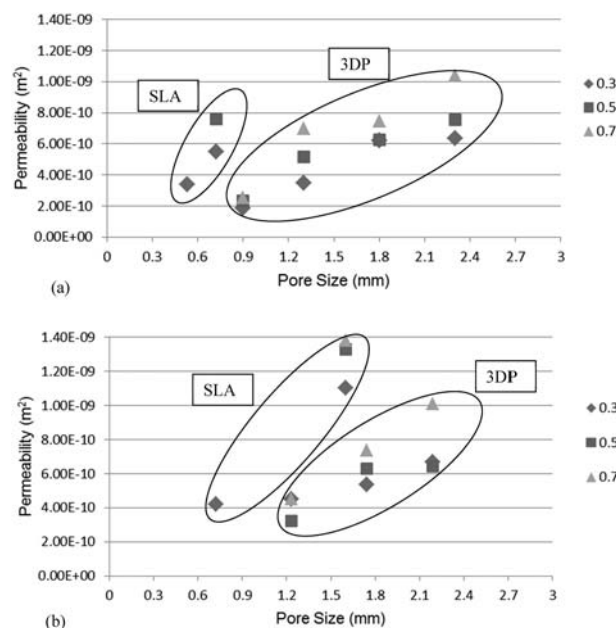
FIGURE 3. Measured permeabilities from (a) cubic and (b) hexagonal structures produced with porosities of 0.3, 0.5, and 0.7 via SLA and 3DP, using water as the testing fluid. [Color figure can be viewed in the online issue, which is available at wileyonlinelibrary.com.]

through structures with increased porosity and pore size. Within the range of pore sizes and porosities measured, pore size had a larger effect on the permeability results than the porosity level. Comparing similar sample types, experimentally measured permeability values were in the range of 2.2 to 3.3 times higher for the glycerol–water solution compared to the less viscous water. This could be
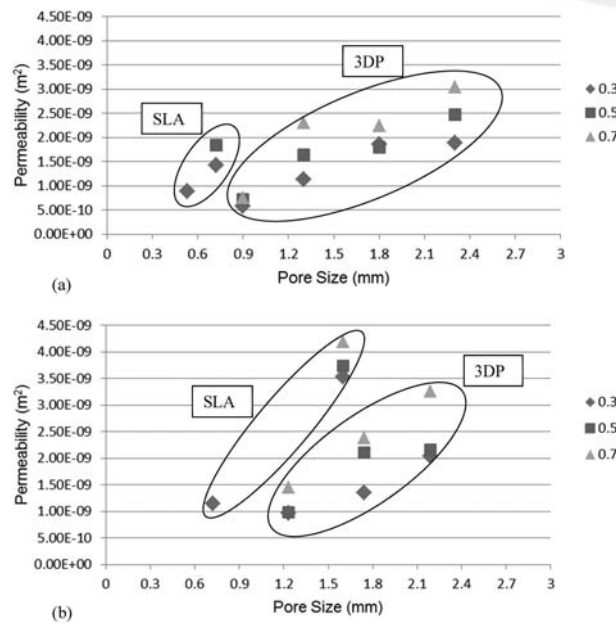

FIGURE 4. Measured permeabilities from (a) cubic and (b) hexagonal structures produced with porosities of 0.3, 0.5, and 0.7 via SLA and 3DP, using glycerol–water as testing fluid. [Color figure can be viewed in the online issue, which is available at wileyonlinelibrary.com.]

TABLE II. Contact Angle Measurements for Different Fluids With 3D Printed and μ-SLA Materials

Media Type	Contact Angle (°) Accura 60 Material	Contact Angle (°) Z-Max Material
Deionized water	64.46	9.51
Tap water	73.5	13.05
Glycerol–water solution (30 m/m %)	70.44	14.51

attributed to higher flow path disorder of the lower viscosity fluid flow through the structures. This range was independent of structure type (hexagonal or cubic). This could be attributed to the higher contact angles with the scaffolds and associated increased hydrophobicity for the more viscous fluid, see Table II Rows 2 and 4. Table II presents the   T2
contact angles determined with the different scaffold materials and fluids. Contact angles for the μ-SLA scaffolds (Accura 60 material) were approximately six times higher, compared to the 3DP scaffolds, indicating their greater degree of hydrophobicity which resulted in higher permeability through the μ-SLA scaffolds compared to the 3DP scaffolds for similar pore size and porosity levels, see Figures 3 and 4. An in-depth review of methods for the evaluation of tissue engineering scaffold permeability has recently been presented.[34]

Mathematical modeling of permeability results

Figure 5 shows the computed permeability for the cubic   F5
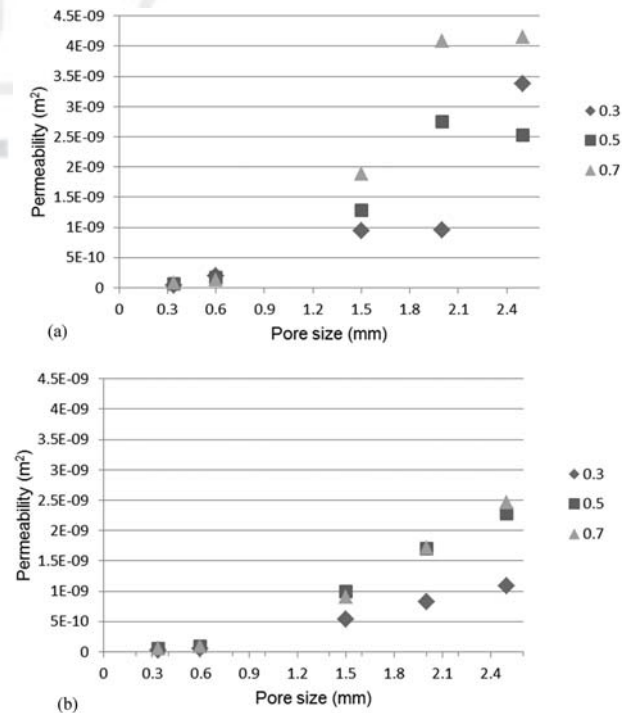and hexagonal structures as calculated using Eq. (5). This

FIGURE 5. Calculated intrinsic permeability for (a) cubic and (b) hexagonal structures having a porosity of 0.3, 0.5, and 0.7. [Color figure can be viewed in the online issue, which is available at wileyonlinelibrary.com.]

TABLE III. Calculated and Measured (With SLA Samples) Permeability Values for Cubic and Hexagonal Structures for 30% Porosity and 0.6 mm Pore Size

Permeability (m^2)	Cubic	Hexagonal
Measured with water	5.49×10^{-10}	4.21×10^{-10}
Measured with glycerol–water	1.43×10^{-9}	1.15×10^{-9}
Theoretical calculation	1.96×10^{-10}	5.17×10^{-11}

formulation of intrinsic permeability derived from the Kozeny–Carman equation is mostly dependent on the solid structural properties, that is, density, specific surface area, and porosity. Fluid densities cancel out and so the results in Figure 5 are independent of fluid type. The calculated permeabilities for the cubic and hexagonal structures ranged from 2.33×10^{-11} m^2 to 4.15×10^{-9} m^2, which encompasses the range of permeabilities measured experimentally. Similar trends in data with pore size and percentage porosity were noted, compared to the measured results. The calculated permeabilities for the cubic structures were 1.1 to 3.8 times higher than for the hexagonal structures. In comparison, the experimental measured permeability values indicated less preference for structure type. Comparing similar sample types, values for the hexagonal structures were in the range of 0.5 to 1.2 times those determined for the cubic structures. This range determined was independent of fluid. The results in Figure 5, and highlighted in Table III, show that the lowest levels of theoretically calculated permeability, which were produced at the lowest pore sizes, were lower than those measured during the experimental

TABLE IV. Comparison of Permeability Values Measured on Different Commercial Artificial Tissue Structures and for Bone Models Tested in This Work

Type	Permeability (m^2)	Ref.
Corals	$0.12–4.46 \times 10^{-9}$	[35]
Collagen–GAG scaffolds	$0.2–0.7 \times 10^{-10}$	[36]
Sponceram®	10^{-9} to 10^{-8}	[37]
SLA and 3D printing	1.84×10^{-10} to 4.19×10^{-9}	This work—experimental

GAG, glycosaminoglycan.

work. This indicates that while Eq. (5) gives a good indication of relative trends between different structures, in order to obtain absolute values which agree more closely with experimental data, the intrinsic formulation should take into account other factors such as pressure drop of fluid across the sample, fluid viscosity and surface energy at the fluid/scaffold interface.

Figure 6 highlights the variation in the specific surface area (S) with pore size and porosity level for the cubic and hexagonal structures. At pore sizes below 1.5 mm the specific surface area of the scaffold sharply increases. With this term effectively being a squared factor in the denominator of Eq. (5), it has the corresponding effect of sharply reducing the permeability at lower pore sizes relative to the experimental results. Similarly, the higher permeability values for pore sizes larger than 1.5 mm can be explained by a sharp decrease in the specific surface area, see Figure 6.

CONCLUSIONS

Combinations of pore sizes ranging from 0.34 mm to 3 mm and porosity content levels from 30% to 70% were investigated in this work. This covers an important range within human bone structure pore sizes in healthy individuals which can range from 0.1 mm to 0.5 mm. Osteoporotic pore size ranges can extend to 3 mm in size and beyond. The resulting range of permeabilities measured was from 1.84×10^{-10} m^2 to 4.19×10^{-9} m^2, which is similar to the range reported in previous studies for analogue and human tissue structures, see Tables IV and V. All experimental results were determined to be highly repeatable. As expected, higher flow
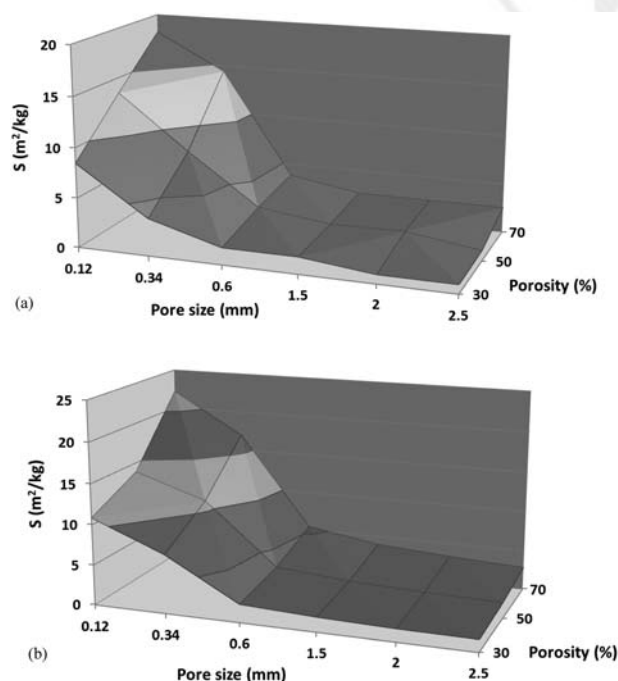

FIGURE 6. The specific surface area (S) compared to the pore size and to the porosity for (a) cubic samples and (b) hexagonal samples. [Color figure can be viewed in the online issue, which is available at wileyonlinelibrary.com.]

TABLE V. Comparison of Permeability Values of Different Bone Types From the Literature and for Bone Models Tested in This Work

Type	Permeability (m^2)	Ref.
Cancellous bone	10^{-11} to 10^{-7}	[32]
Human calcaneal trabecular bone	0.4×10^{-9} to 10.97×10^{-9}	[8]
Human proximal femur, cancellous bone	10^{-11} to 10^{-8}	[2]
SLA and 3D printing	2.33×10^{-11} to 4.15×10^{-9}	This work—theory
SLA and 3D printing	1.84×10^{-10} to 4.19×10^{-9}	This work—experimental

rates and permeabilities were recorded for larger porosity content levels and pore sizes. This follows also from the theoretical calculations where increased pore size provided a decrease in specific surface area which in turn results in increased permeability, see Eq. (5).

The experimental permeability measurements from water–glycerol were 2.2 to 3.3 times higher than for water. This range was the same for both structure morphologies, cubic and hexagonal. This difference in permeabilities can be attributed to the different surface energies at the fluid/scaffold interface. Contact angles for μ-SLA scaffold material were in the range of five to seven times those of the 3DP scaffold materials. Higher hydrophobicity of the μ-SLA scaffold material could therefore be expected to result in increased permeability. From Eq. (2), formulation for intrinsic permeability, increased viscosity of the water–glycerol solution can also be seen to result in increased permeability.

The theoretical calculated permeability through the cubic structures was determined to be 1.1 to 3.8 times higher compared to that through the hexagonal structures. However, the experimental results showed no determinable effect on permeability, for either fluid, of pore morphology between the cubic and hexagonal structures. This discrepancy between experiment and theory could be partly due to an insufficient number of lattice cells having been tested during the experimental work. The theoretical calculation however using Eq. (5) does not take into account pressure drop of fluid across the sample, fluid viscosity, or surface energy at the fluid/scaffold interface. While Eq. (5) provides more comprehensive analysis of the effect of scaffold structure on permeability, Eq. (2) accounts for some of these latter mentioned parameters. A new model therefore combining the benefits of these two equations is suggested from this work in order to determine absolute permeability values.

The predominant factor experimentally and theoretically affecting permeability values was the pore size. Viscosity was found to be the next most influential factor followed by level of porosity. Increased pore size, viscosity, and porosity resulted in the highest permeability values. The work presented in this article indicates that the fluid viscosity and corresponding surface energy at the fluid–solid interface have a significant influence on permeability. Specifically, higher viscosity and surface energy, within the bounds of the values examined in this study, resulted in significantly higher permeability values. Structure morphology along the primary axis, in terms of the cubic and hexagonal structures evaluated, were not found to have a significant effect on permeability.

When designing bone scaffolds for use during orthopedic surgery, biocompatibility and an ability to withstand the local loading requirements are primary initial considerations. For longer term success of the implant, good permeability of the scaffold is critical to allow for inflow of cells and nutrients, as well as for waste product transfer. The results of this article show that in order to achieve good permeability, the pore size, porosity level, and material surface energy are primary design parameters that must be controlled. From the clinical viewpoint, the results presented here also illustrate how the variations in patient's blood viscosity can be extremely important in allowing for permeability through the bone and scaffold structures. Careful consideration and further research should therefore focus on the effects on viscosity of the use of procoagulopathic agents or even the short term administration of anticoagulants such as heparin in an effort to aid patency of these channels.

REFERENCES

1. Cheung HY, Lau KT, Lu TP, Hui D. Compos Part B: Eng 2007;38: 291–300.   **AQ5**
2. Shimko DA, Nauman EA, J Biomed Mater Res Part B: Appl Biomater 2007;80B:360–369.
3. Shimko DA, Shimko VF, Sander EA, Dickson KF, Nauman EA. J Biomed Mater Res Part B: Appl Biomater 2005;73B:315–324.
4. Ochoa I, Sanz-Herrera JA, Garcia-Aznar JM, Doblare M, Yunos DM, Boccaccini AR. J Biomech 2009;42:257–260.
5. Dhandayuthapani B, Yoshida Y, Maekawa T, Kumar D. Int J Polym Sci 2011;2011:19. doi:10.1155/2011/290602.
6. Jones JR, Poologasundarampillai G, Atwood RC, Bernard D, Lee PD. Biomaterials 2007;28:1404–1413.
7. Chor MV, Li W. Meas Sci Technol 2007;18:208–216.
8. Grimm MJ, Williams JL. J Biomech 1997;30:743–745.
9. Botchwey EA, Dupree MA, Pollack SR, Levine EM, Laurencin CT. J Biomed Mater Res Part A 2003;67A:357–367.
10. Agrawal CM, McKinney JS, Lanctot D, Athanasiou KA. Biomaterials 2000;21:2443–2452.
11. Al-Munajjed AA, Hien M, Kujat R, Gleeson JP, Hammer J. J Mater Sci: Mater Med 2008;19:2859–2864.
12. Karande TS, Ong JL, Agrawal CM. Ann Biomed Eng 2004;32: 1728–1743.
13. Li SH, de Wijn JR, Li JP, Layrolle P, de Groot K. Tissue Eng 2003; 9:535–548.
14. Beno T, Yoon YJ, Cowin SC, Fritton SP. J Biomech 2006;39:2378–2387.
15. Kohles SS, Roberts JB, Upton ML, Wilson CG, Bonassar LJ, Schlichting AL. J Biomech 2001;34:1197–1202.
16. Knothe Tate ML, Knothe U. J Biomech 2000;33:247–254.
17. Brennan S, Brabazon D, O'Byrne J. J Bone Joint Surg 2011;93B: 755–759.
18. O'Brien F, Harley B, Waller M, Yannas I, Gibson L, Prendergast P. Technol Health Care 2007;15:3–17.
19. Gibson LJ, Ashby MF. Cellular Solids: Structure and Properties. Cambridge: Cambridge University Press; 1999.
20. Malachanne E, Dureisseix D, Ca adas P, Jourdan F. J Biomech 2008;41:721–725.
21. Swider P, Conroy M, Pédrono A, Ambard D, Mantell S, Sballe K, Bechtold JE. J Biomech 2007;40:2112–2118.
22. Haugen H, Will J, Kohler A, Hopfner U, Aigner J, Wintermantel E. J Eur Ceram Soc 2004;24:661–668.
23. Eosoly S, Brabazon D, Lohfeld S, Looney L. Selective laser sintering of hydroxyapatite/poly-ε-caprolactone scaffolds. Acta Biomater 2010;6:2511–2517.
24. Eosoly S, Lohfeld S, Brabazon D. Effect of hydroxyapatite on biodegradable scaffolds fabricated by SLS. Key Eng Mater 2009;396-398:659–662.
25. Szucs T, Brabazon D. Effect of saturation and post processing on 3D printed calcium phosphate scaffolds. Key Eng Mater 2009;396-398:663–666.
26. Lipowiecki M, Ryvolova M, Tottosi A, Naher S, Brabazon D. Permeability of rapid prototyped artificial bone scaffold structures. Adv Mater Sci Res 445;2012:607–612.
27. Lipowiecki M, Brabazon D. Design of bone scaffolds structures for rapid prototyping with increased strength and osteoconductivity. Adv Mater Res 2010;83-86:914–922.
28. Rosenson RS, McCormick A, Uretz EF. Clin Chem 1996;42:1189–1195.
29. Lowe GD, Drummond MM, Lorimer AR, Hutton I, Forbes CD, Prentie CR, Barbenel JC. Br Med J 1980;280:673.

30. Chapuis RP, Aubertin M. Technical Report EPM-RT-2003 03, École Polytechnique, Montréal, Quebec; 2003.

31. Steiakakis E, Gamvroudis C, Alevizos G. Kozeny–Carman equation and hydraulic conductivity of compacted clayey soils. Geomaterials 2012;2:37–41.

32. Syahroma A, Kadirb MRA, Abdullahc J, Öchsnera A. Permeability studies of artificial and natural cancellous bone structures. Med Eng Phys 2013;35:792–799.

33. Truscello S, Kerckhofs G, Van Bael S, Pyka G, Schrooten J, Van Oosterwyck H. Prediction of permeability of regular scaffolds for skeletal tissue engineering: A combined computational and experimental study. Acta Biomater 2012;8:1648–1658.

34. Pennella F, Cerino G, Massai D, Gallo D, Labate GF, Schiavi A, Deriu MA, Audenino A, Morbiducci U. A survey of methods for the evaluation of tissue engineering scaffold permeability. Ann Biomed Eng 2013;4:2027–2041.

35. Wu YC, Lee TM, Chiu KH, Shaw SY, Yang CY. J Mater Sci: Mater Med 2009;20:1273–1280.

36. Tierney CM, Haugh MG, Liedl J, Mulcahy F, Hayes B, O'Brien FJ. J Mech Behav Biomed Mater 2009;2:202–209.

37. Sanz-Herrera JA, Kasper C, van Griensven M, Garcia-Aznar JM, Ochoa I, Doblare M. J Biomed Mater Res Part B: Appl Biomater 2008;87B:42–48.

AQ1: Kindly check whether the short title is OK as given.

AQ2: Please confirm that all author names are OK and are set with first name first, surname last.

AQ3: Superscript "1" linked to author "Marcin Lipowiecki" has been deleted, as no significance was provided. Please check.

AQ4: Please provide department name (if any) for affiliation 5.

AQ5: Please provide article title for Refs. 1–18, 20–22, 28, 29, 35–37.

AQ6: Please confirm whether the color figures should be reproduced in color or black and white in the print version. If the color figures must be reproduced in color in the print version, please fill the color charge form immediately and return to Production Editor. Or else, the color figures for your article will appear in color in the online version only.